Quenched optical transmission in ultrathin subwavelength plasmonic gratings

G. D'Aguanno,[1,2,*] N. Mattiucci,[1,2] A. Alù,[3] and M. J. Bloemer[2]

[1]*Nanogenesis Division, AEgis Technologies, Nanogenesis Division, 410 Jan Davis Drive, Huntsville, Alabama 35806, USA*

[2]*Department of the Army, Charles M. Bowden Facility, Building 7804, Research Development and Engineering Command, Redstone Arsenal, Alabama 35898, USA*

[3]*Department of Electrical and Computer Engineering, University of Texas at Austin, Austin, Texas 78712, USA*

(Received 3 November 2010; revised manuscript received 13 December 2010; published 27 January 2011)

We discuss the optical properties of one-dimensional ultrathin subwavelength, metallic gratings under transverse magnetic excitation, with particular attention to the phenomenon of quenched transmission, recently highlighted in several optical experiments. In particular, we consider a grating with thickness comparable to or less than the metal skin depth, showing how the geometrical properties of the grating can dramatically modify its transmission properties, often in a counterintuitive way. We study the role played by short-range and long-range surface plasmons (SPs) and localized SP resonances, showing that quenched transmission must be ascribed to localized resonance effects, while long-range and short-range SPs play only a marginal role in this anomalous effect.

DOI: 10.1103/PhysRevB.83.035426 PACS number(s): 42.25.−p

I. INTRODUCTION

The optical properties of subwavelength one-dimensional (1D) and two-dimensional (2D) metallic gratings have been the subject of intense investigation since the beginning of last century, when Wood noted anomalies in the distribution of the diffracted orders from 1D metallic gratings under transverse magnetic (TM) light excitation.[1] In particular, the phenomenon of extraordinary optical transmission (EOT) in 1D and 2D subwavelength apertures and gratings has been widely analyzed in the last 15 years: detailed and complete reviews of the main progresses in the field may be found in Refs. 2 and 3. In EOT phenomena, more light passes through the subwavelength apertures of a periodically perforated, thick, opaque, metallic screen than one might expect based on simple geometrical considerations,[2,3] implying that the transmission efficiency, i.e., the transmitted power flux normalized to the flux incident on the surface of the holes, may exceed unity. This resonant phenomenon can also be explained in the framework of the physics of guided mode resonances,[4–6] or of leaky modes supported by the grating.[7,8] In this framework, it should be noted that, although EOT has received a great deal of attention in the last decade, some of its aspects have been widely used by microwave and optical engineers, in particular referring to the concept that metal gratings with subwavelength periodicity can act as anisotropic conductors, directive radiators, or very efficient light polarizers (the so-called wire-grid polarizers).[9–12]

In the above-mentioned works attention has been focused on thick optical gratings, with thickness larger than the metal skin depth, for which the metal is inherently opaque. For example, the complex refractive index of silver at $\lambda = 600$ nm is $n = 0.124 + i3.732$,[13] which results in a skin depth of approximately 25 nm. Recently, however, a new counterintuitive phenomenon has been put forward, analyzing the electromagnetic properties of subwavelength metallic gratings with thickness comparable to or less than the metal skin depth. In particular, it has been pointed out that in this regime a phenomenon somewhat complementary to EOT may take place.[14–16] While one might naively expect that such ultrathin gratings could be semitransparent to the incident radiation, it has been recently noticed that under TM excitation the transmission from the structure may be resonantly suppressed, with an anomalous increase in absorption, despite the ultrathin nature of the grating. Such quenched transmission and anomalous enhanced absorption has been studied for 1D, ultrathin, metallic gratings both from the theoretical[14] and experimental[15] points of view. In Ref. 16, the suppressed transmission through a ultrathin metal film perforated with an array of subwavelength holes has been experimentally verified. In this context, it is also worthwhile mentioning the work in Ref. 17, where transmission through an ultrathin metal film perforated with a 2D hole array was numerically studied. Due to the specific transverse magnetic polarization preference, it has been speculated that this phenomenon might be associated with the presence of surface plasmons traveling along the grating layer.

In this work, we analyze in more detail the counterintuitive phenomenon of quenched transmission and report our analysis of the optical properties of 1D, ultrathin, subwavelength metallic gratings under TM excitation. We focus on the role played by short-range and long-range surface plasmons (SPs) and localized plasmon resonances. Our analysis shows that the quenched transmission effect must be ascribed to localized surface plasmons, while planar SPs play only a marginal role. This holds true for both wide and narrow slits.

II. RESULTS AND DISCUSSION

The geometry under analysis is depicted in Fig. 1(a). A plane, monochromatic, TM-polarized wave is incident on a self-standing grating made of silver and placed *in vacuo* (substrate effects will be discussed later in the paper). The dispersion of silver is taken from Ref. 13 and it is reported in Fig. 1(b). Note that the oscillations in the real part of the permittivity in the long-wavelength region result from the overlap of data points obtained from different experimental groups.[13] The transmission (T), reflection (R), and absorption (A) are

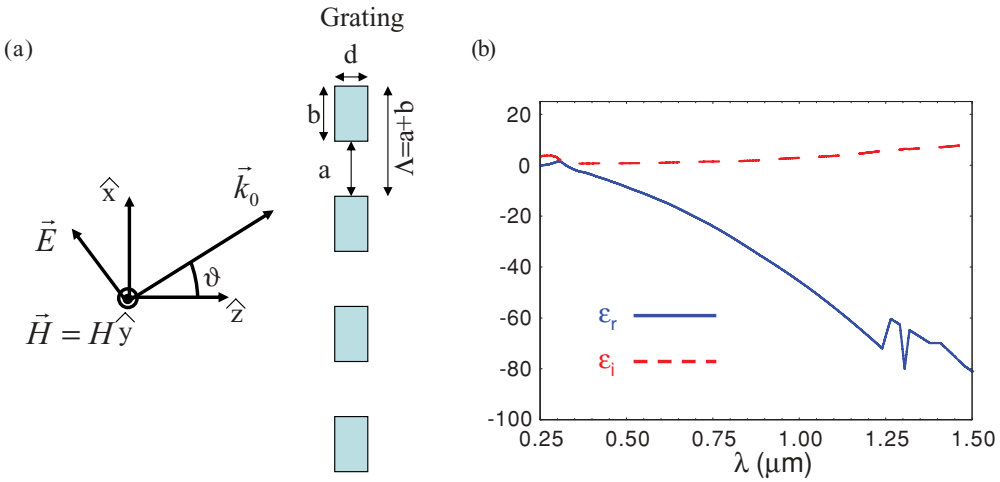

FIG. 1. (Color online) (a) Metallic grating made of silver with grating thickness d, slit aperture a, and grating period $\Lambda = a + b$ where b is the length of the metal in the elementary cell. The incident field is a plane, monochromatic, TM-polarized wave where $k_0 = 2\pi/\lambda$ is the wave vector, λ is the wavelength, and ϑ is the incident angle. In this case we consider air as the incident and the output medium. The Cartesian right-handed system (x,y,z) has the z coordinate in the propagation direction and the x coordinate along the periodicity of the grating. The y coordinate is the direction along which the magnetic field H is polarized. The input grating surface is located at $z = 0$ and the output surface at $z = d$. (b) Real (ε_r) and imaginary (ε_i) parts of the electric permittivity of silver from data reported in Ref. 13.

calculated using the Fourier-modal-method technique.[6,18–20] In particular, for TM polarization we have[6]

$$T = \frac{n_{\text{in}}}{k_0 n_{\text{out}}^2 \cos\vartheta} \sum_m |t_m|^2 \text{Re}\left[\sqrt{n_{\text{out}}^2 k_0^2 - \alpha_m^2}\right], \quad (1a)$$

$$R = \frac{1}{k_0 n_{\text{in}} \cos\vartheta} \sum_m |r_m|^2 \text{Re}\left[\sqrt{n_{\text{in}}^2 k_0^2 - \alpha_m^2}\right], \quad (1b)$$

$$A = 1 - R - T, \quad (1c)$$

where $k_0 = 2\pi/\lambda$ is the vacuum wave vector, n_{in} and n_{out} are respectively the refractive indices of the input and output

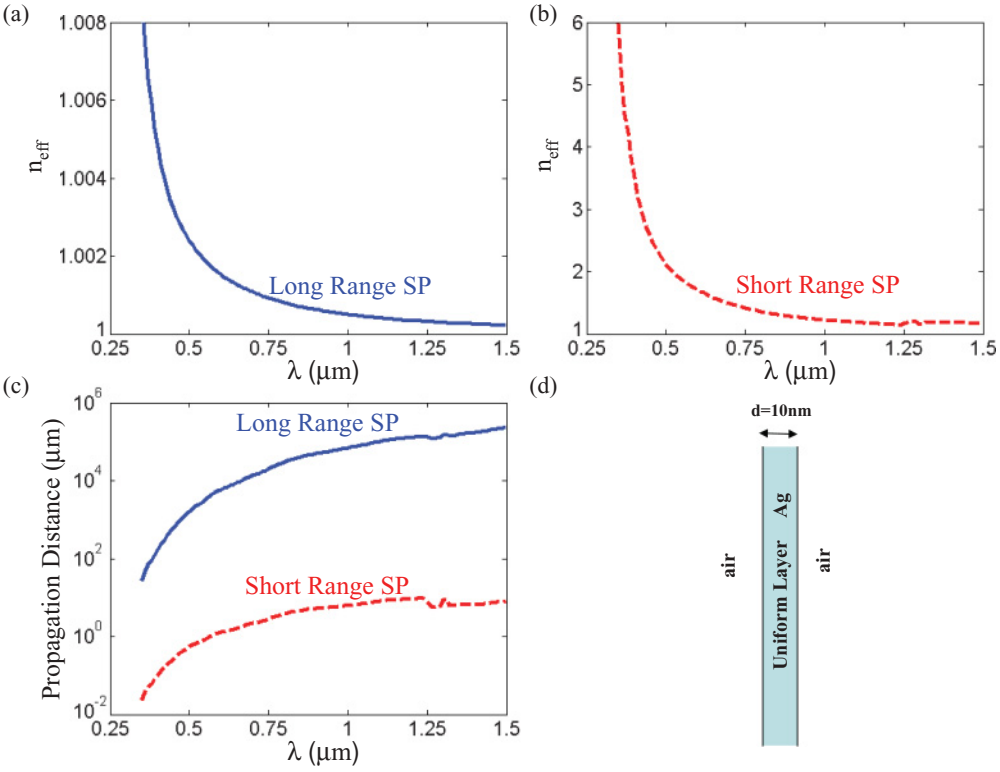

FIG. 2. (Color online) (a) Real part of the effective index of the long-range SP vs wavelength for a structure air/Ag(10 nm)/air. (b) Real part of the effective index of the short-range SP vs wavelength. (c) Propagation distance of the long-range SP (continuous line) and of the short-range SP (dashed line) vs wavelength. (d) Schematic representation of a structure air/Ag(10 nm)/air.

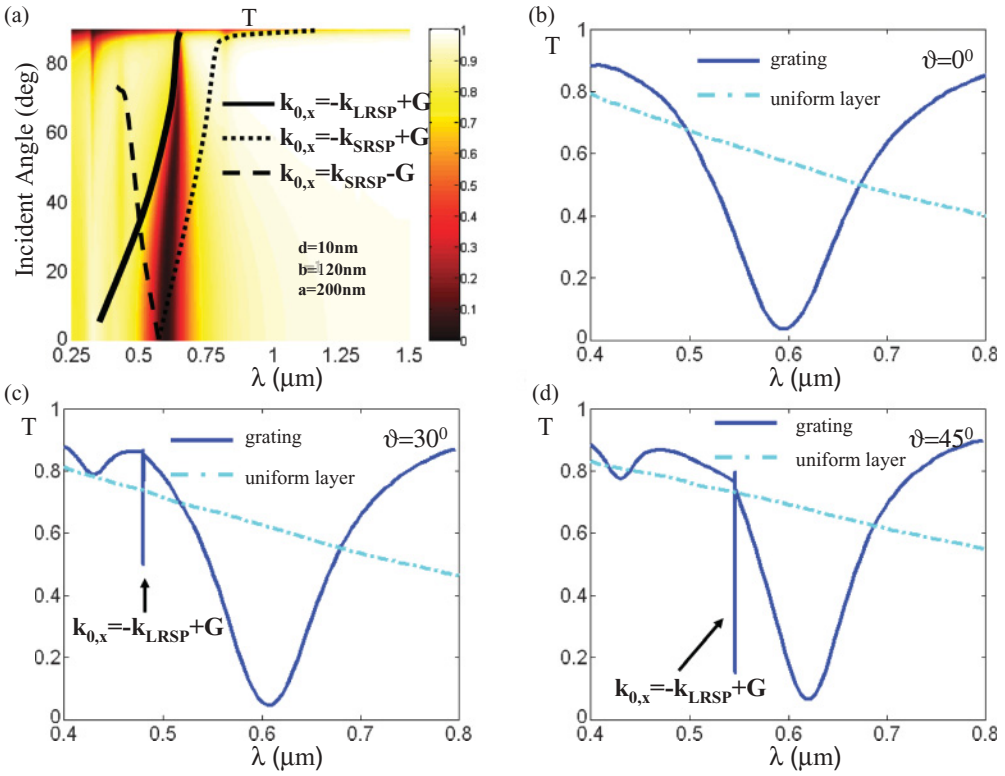

FIG. 3. (Color online) (a) T vs incident wavelength (λ) and incident angle (ϑ) for a grating with thickness $d = 10$ nm, slit aperture $a = 200$ nm, and period $\Lambda = a + b = 320$ nm. Superimposed is the dispersion of the photon-LRSP and photon-SRSP coupling as calculated from Eqs. (3). The continuous line corresponds to the photon-LRSP coupling mediated through G; the dotted and dashed lines correspond the photon-SRSP coupling mediated respectively through $+G$ and $-G$. (b) T vs incident wavelength (λ) at normal incidence ($\vartheta = 0^\circ$) for the grating (continuous line) and for the uniform layer (dash-dotted line). (c) T vs incident wavelength (λ) at $\vartheta = 30^\circ$ for the grating (continuous line) and for the uniform layer (dash-dotted line). The arrow indicates the spike (anomaly) in the transmission of the grating, which is in correspondence with the photon-LRSP coupling mediated through $+G$. (d) Same as (c) at $\vartheta = 45^\circ$.

medium ($n_{\text{in}} = n_{\text{out}} = 1$ in our case), ϑ is the incident angle of the incoming wave on the grating, t_m and r_m are respectively the complex transmission and reflection coefficients of the mth diffracted order, Re indicates the real part, and finally α_m is the generalized transverse wave vector:

$$\alpha_m = k_0 n_{\text{in}} \sin\vartheta + \frac{2m\pi}{\Lambda}, \quad m = 0, \pm 1, \pm 2, \ldots, \pm N. \qquad (2)$$

The number N of diffraction orders retained in our numerical calculations is specified by the sampling of the transverse profile of the electric permittivity function $\varepsilon(x)$ according to the Nyquist-Shannon sampling theorem.[21] In particular, if dx is the sampling step, the number of retained diffraction orders is $N = \Lambda/(2dx)$. In our calculations a sampling step $dx = 4$ nm for a period $\Lambda = 320$ nm, corresponding to $N = 40$, already ensures excellent convergence of the solution. T, R, and A in Eqs. (1a)–(1c) represent respectively the transmission, reflection, and absorption coefficients of the elementary cell of the grating, normalized to the total incident power on the elementary cell of the grating, and therefore they are always smaller than or equal to 1 for visible incidence angles, due to energy conservation. This is different from the commonly used transmission coefficients in EOT experiments, which normalize the power with respect to the impinging flux on the slit area.[3]

Here we are interested in studying the electromagnetic properties of the grating in a regime where its thickness d is comparable to or less than the skin depth in the metal. As we have already mentioned in the Introduction, at 600 nm the skin depth of the silver is ~25 nm; therefore we choose a grating thickness $d = 10$ nm. This value is currently within the limits of thermal evaporation or sputtering fabrication techniques[22] and, more importantly, it still allows a classical description of the wave interaction with the metal, for which quantum effects are negligible.[23] While the percolation threshold for Ag films is highly dependent on the fabrication details, we note that Maaroof and Sutherland[24] measure a percolation threshold of 4 nm for Ag films fabricated by dc magnetron sputtering and observe smooth continuous films at 9 nm thickness. In addition, Okamoto *et al.*[25] observe smooth continuous Ag films at a thickness of 6 nm for thermally evaporated films. Recently, slight modifications to the bulk properties of Ag have been reported for coupled Ag strips.[26] Nevertheless, the use of a more refined dispersion model does not significantly affect the following discussions and for this reason we will use in our calculations the bulk permittivity of Ag.

We start our analysis by describing in Fig. 2 the planar SP modes of a uniform, 10 nm Ag layer embedded in air. As is well known,[27–29] in a thin metal layer (say, less than 40 nm) embedded in a symmetric environment, the typical

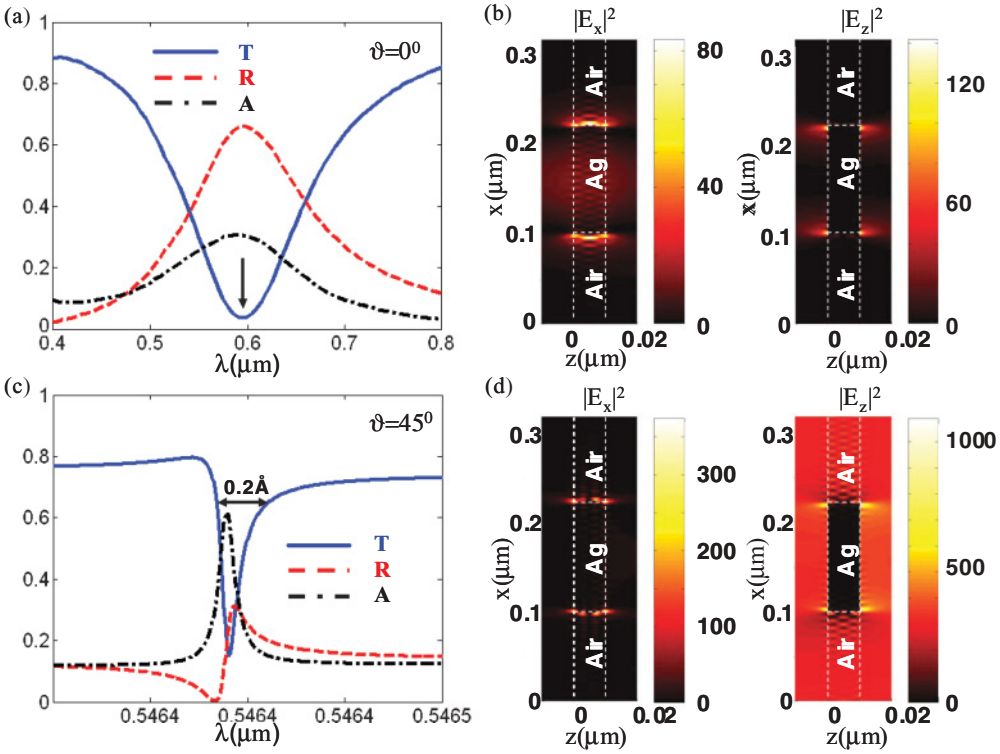

FIG. 4. (Color online) (a) Transmission (T), reflection (R), and absorption (A) at normal incidence vs incident wavelength (λ) for the grating described in Fig. 3. The arrow indicates the transmission minimum located at $\lambda = 595$ nm. (b) Corresponding electric field localizations over the elementary cell of the grating at $\lambda = 595$ nm. (c) Transmission (T), reflection (R), and absorption (A) at 45° incidence vs incident wavelength (λ) for the grating described in Fig. 3. This extremely sharp resonance (0.2 Å) is the magnification of the resonance already shown in Fig. 3(d) that is due to the photon-LRSP coupling. (d) Electric field localizations at the transmission minimum.

dispersion of the single interface SP splits into two branches which correspond to guided modes with opposite properties, commonly called *long-range* and *short-range* plasmons. These findings are confirmed by the dispersion properties reported in Fig. 2.

In Figs. 2(a) and 2(b), the dispersion of the effective indices for the long-range and short range plasmons are shown, respectively, and in Fig. 2(c) their respective propagation distances are shown. Note that the long-range SP has an effective index close to 1 and long propagation distances ($\sim 10^5$ μm), which is an indication that the electric field is mainly concentrated outside the metal layer, suffering therefore only moderate Ohmic losses.[27,28] On the contrary, the short-range SP has a high effective index and most of the electric field is concentrated in the metal layer, causing strong Ohmic losses and short propagation distances (~ 1 μm). Both short-range and long-range plasmons on a uniform plasmonic layer can couple with the incident light through the reciprocal lattice vector in the case of a grating. This photon-plasmon coupling is described by the following equation which, as in the standard grating coupler, represents the condition of transverse momentum conservation between the incident field and the guided mode mediated through the reciprocal lattice vector of the grating:[30,31]

$$3k_{0,x} = |\pm k_{\mathrm{LRSP/SRSP}} \mp mG|, \quad m = 0,1,2,\ldots, \qquad (3a)$$

where $k_{0,x} = k_0 \sin\vartheta$ is the transverse momentum of the incident field according to the geometry described in Fig. 1, ϑ is the incident angle, $k_0 = 2\pi/\lambda$ the incident wave vector, λ the incident wavelength, $k_{\mathrm{LRSP/SRSP}} = k_0 n_{\mathrm{eff}}$ is the wave vector of the long-range (LR) or short-range (SR) SP, n_{eff} is the corresponding real part of the effective index, $G = 2\pi/\Lambda$ is the reciprocal lattice vector of the grating, and m is an integer that stands for the different diffracting orders of the grating. Equation (3a) can also be recast in an equivalent form that involves directly the incident angle ϑ, the grating period Λ, the incident wavelength λ, and the effective index n_{eff}:

$$\sin(\vartheta) = \left|\pm n_{\mathrm{eff}} \mp m\frac{\lambda}{\Lambda}\right|, \quad m = 0,1,2,\ldots. \qquad (3b)$$

Once the incident wavelength, the grating period, and the effective index of the guided mode are fixed, Eq. (3a), or equivalently Eq. (3b), determines the coupling angle ϑ. In order to investigate how this coupling affects the transmission properties of the grating, in Fig. 3(a) we report the transmission (T) in the plane (λ, ϑ) for a silver grating of thickness $d =$ 10 nm, slit aperture $a = 200$ nm, width of the metal in the elementary cell, $b = 120$ nm, and period $\Lambda = a + b = 320$ nm. Note that here we consider a grating with wide slits, in other words the air filling fraction of the grating is $a/\Lambda \sim 62\%$, i.e., air is the prevalent material of the grating.

As outlined in the Introduction, we indeed observe a general resonant suppression of transmission at a wavelength of 600 nm. This transmission drop, which remains constant in frequency over a wide range of incident angles, is very counterintuitive, since the grating thickness is well below

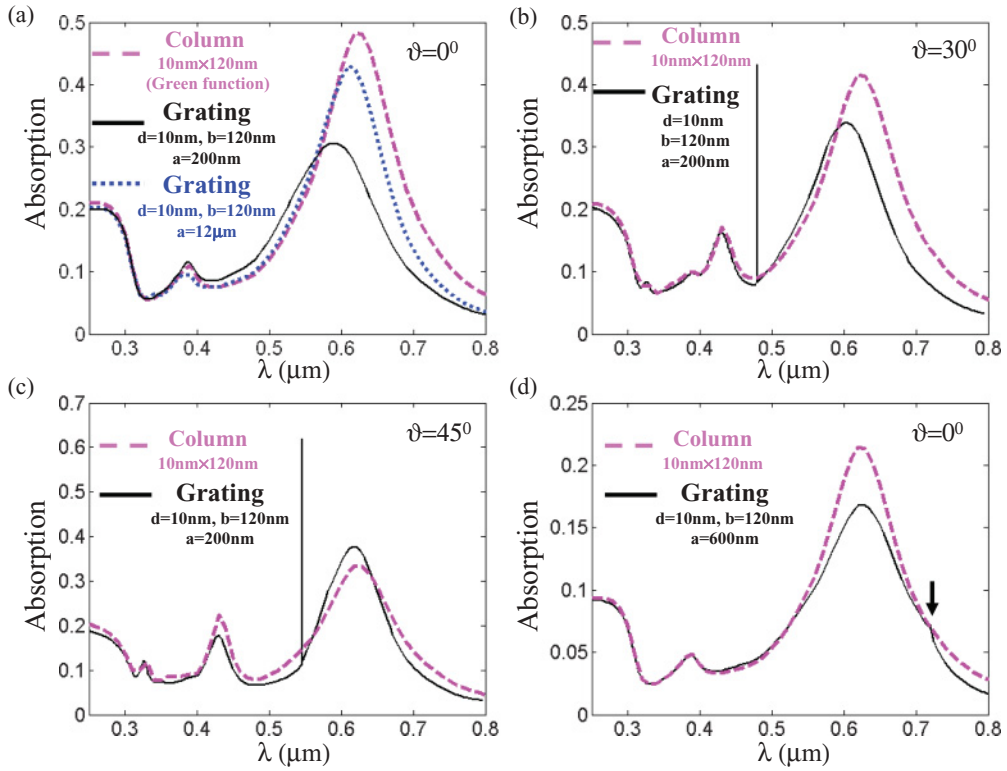

FIG. 5. (Color online) (a) Normalized absorption (A) vs incident wavelength at normal incidence calculated according to Eqs. (1) for the grating (continuous line) and according to Eq. (4) for a single column (dashed line) whose dimensions b and d are the same as those of the grating. The grating is the one described in Fig. 3. The calculation for the single column has been performed using a rigorous Green's function approach. For comparison we have also reported (dotted line) the normalized absorption of a grating with period much longer than the incident wavelength. The spacing between the columns is 12 μm. As expected, in this case the absorption resonance of the grating is very close to the absorption resonance of the single column. (b) Same as in (a) at 30° incidence for a single column and a grating with $a = 200$ nm. (c) Same as in (b) at 45° incidence. (d) Absorption at 45° for a single column and a grating with $a = 600$ nm. In (d) the arrow indicates the position of a small cusp in the absorption of the grating located at $\lambda = \Lambda = 720$ nm, which corresponds to the Rayleigh condition.

the silver skin depth and we have additionally opened wide vacuum gaps in the grating. In order to better highlight the resonant nature of the quenched transmission, in Fig. 3(b) we show the transmission of the grating at normal incidence (continuous line) and compare it with the transmission of a uniform layer of silver with the same thickness (dash-dotted line).

We investigate now the connection between the quenched transmission frequency and the photon-LRSP or photon-SRSP coupling. To this end, Fig. 3(a) shows the dispersion of photon-LRSP and photon-SRSP coupling, as described by Eqs. (3). The continuous line corresponds to the photon-LRSP coupling mediated through G, while the dotted and dashed lines correspond to the photon-SRSP coupling respectively mediated through $+G$ and $-G$. There are two important features that appear immediately at a first inspection of Fig. 3(a). At normal incidence the SRSP resonance overlaps the transmission minimum, giving the impression that SRSPs could be responsible for the low transmission. However, at higher angles photon-SRSP coupling seems to have no effect on the quenched transmission resonance frequency. This is not surprising after all: it can be explained by recalling that the propagation length of the SRSP is only ~ 1 μm [see Fig. 2(c)], which means that the SRSP can propagate for just a few elementary cells of the grating. Indeed, at the transmission minimum ($\lambda = 595$ nm) the propagation length (L_D) for the SRSP calculated in Fig. 2(c) is $L_D \cong 620$ nm, which means a propagation distance approximately equal to one wavelength. Evidently this fact prevents any efficient photon-SRSP coupling, as such efficient coupling may take place only when the plasmon propagation length spans many wavelengths. In other words, the SRSP is too lossy in this case to claim any effective coupling with the grating. This is obviously not the case for the LRSP, which has a propagation distance of $\sim 10^5$ μm [see Fig. 2(c)], encompassing hundreds of thousands of elementary cells of the grating.

Another feature coming to our attention by observing Fig. 3(a) is that the photon-LRSP coupling (continuous line) seems to shape the frequency of the quenched transmission at low wavelengths and high incident angles. Let us closely analyze how the photon-LRSP coupling affects the zone of quenched transmission. In Figs. 3(c) and 3(d) we show T vs λ for incident angles of 30° and 45° in the case of the grating (continuous line) and uniform layer (dot-dashed line). The figures clearly show that the photon-LRSP coupling is responsible for sharp transmission spikes. These anomalies are characterized by extremely narrow resonances ($\sim$0.2 Å), somewhat similar to Wood's anomalies.[1] The figures should

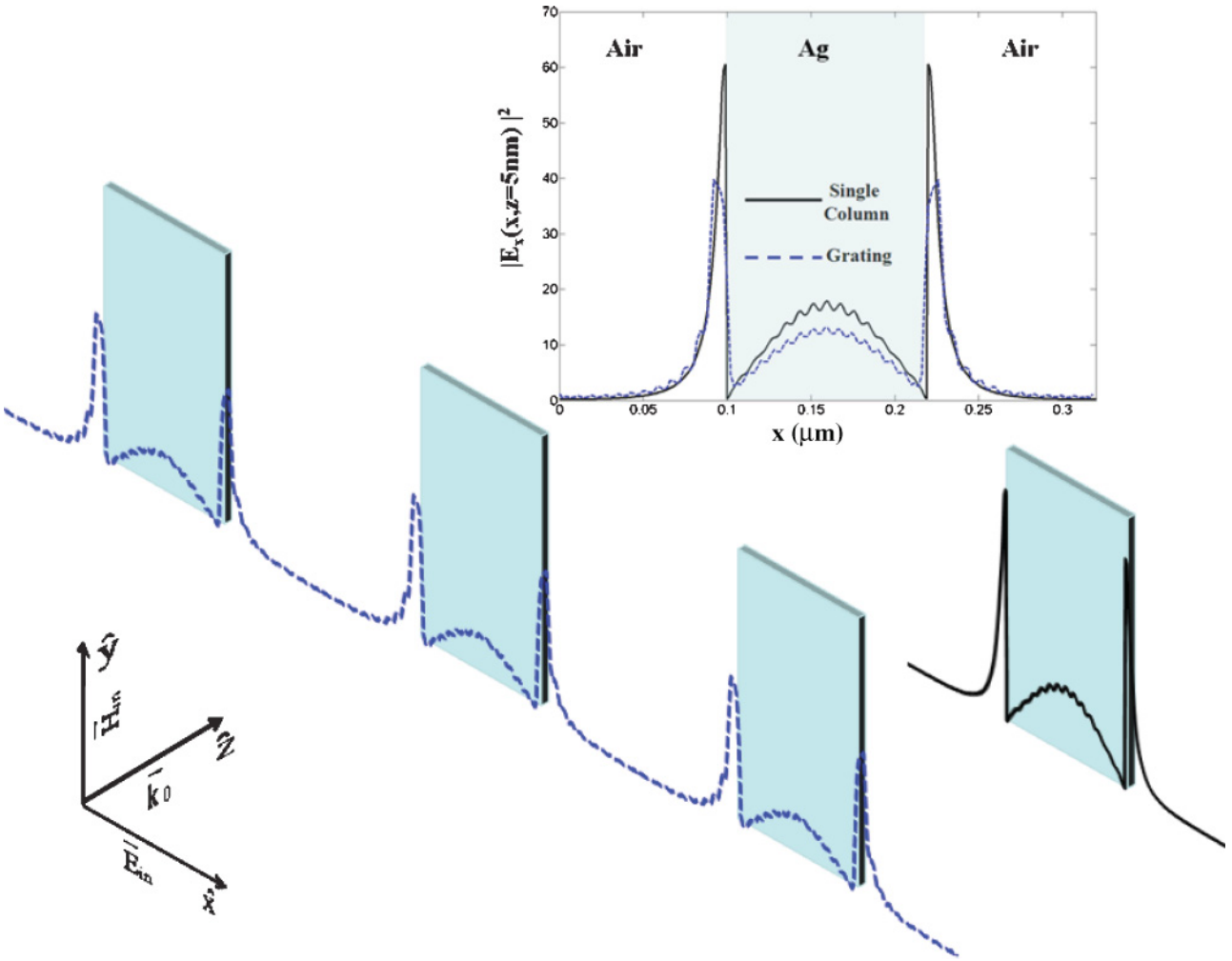

FIG. 6. (Color online) $|E_x|^2$ calculated along the x axis at the center of the grating (dashed line) and at the center of a single column (continuous line) for a normally incident plane wave with $\lambda = 595$ nm. The grating is the same as the one described in Fig. 3 and the single column is the same as the one described in Fig. 5(a).

also make clear that the wideband resonance centered at 600 nm, which is responsible for the quenched transmission, is actually not linked to the LRSP-photon coupling, the latter giving just extremely sharp, narrowband resonances (anomalies) that may be considered local perturbations to the overall shape of the wideband resonance of the quenched transmission. To confirm this finding, in Fig. 4 we compare the main near-field properties of the wideband resonance with those of the narrowband resonance.

Figure 4(a) shows the wideband resonance responsible for quenched transmission and Fig. 4(b) the corresponding electric field localizations at the transmission minimum. Figure 4(c) shows the peculiar properties of the narrowband resonance due to the photon-LRSP coupling and Fig. 4(d) the electric field localizations at the transmission minimum. The different nature of the two resonances is evident if we look at their respective field localizations, but also if we look at the different nature of the associated resonances in reflection. The wideband resonance has a typical quasi-Lorentzian shape in reflection [see Fig. 4(a)], while the narrowband resonance has a typical Fano shape[32,33] [see Fig. 4(c)]. Regarding the electric field localization properties of this grating, it is evident in Fig. 4(b) that the electric field localization for the wideband quenched transmission resembles that of an electric dipole along the x axis, while the electric field localization for the narrowband quenched transmission shown in Fig. 4(d) is typical of a LRSP coupled with the grating. Note in particular in Fig. 4(d) how the z component of the electric field is dominant with respect to the x component, and that it is localized mainly in air; this is another peculiar characteristic of a LRSP mode guided along the x direction.

It is now left to address the last and most important question regarding the nature of the wideband resonant suppression of transmission in ultrathin gratings. Up to now, we have ruled out SRSPs because of their extremely short propagation length and LRSPs because we have demonstrated that they actually give rise to extremely sharp resonances, more similar to Wood's anomalies. To the end of further understanding the nature of this quenched transmission, in Fig. 5 we report the absorption (A) of our grating as calculated from Eqs. (1). and compare it with the absorption of a *single* silver column of rectangular section whose dimensions b and d are the same as in the grating, and also with a grating with very large period. Note that in our 1D geometry (see Fig. 1) the grating

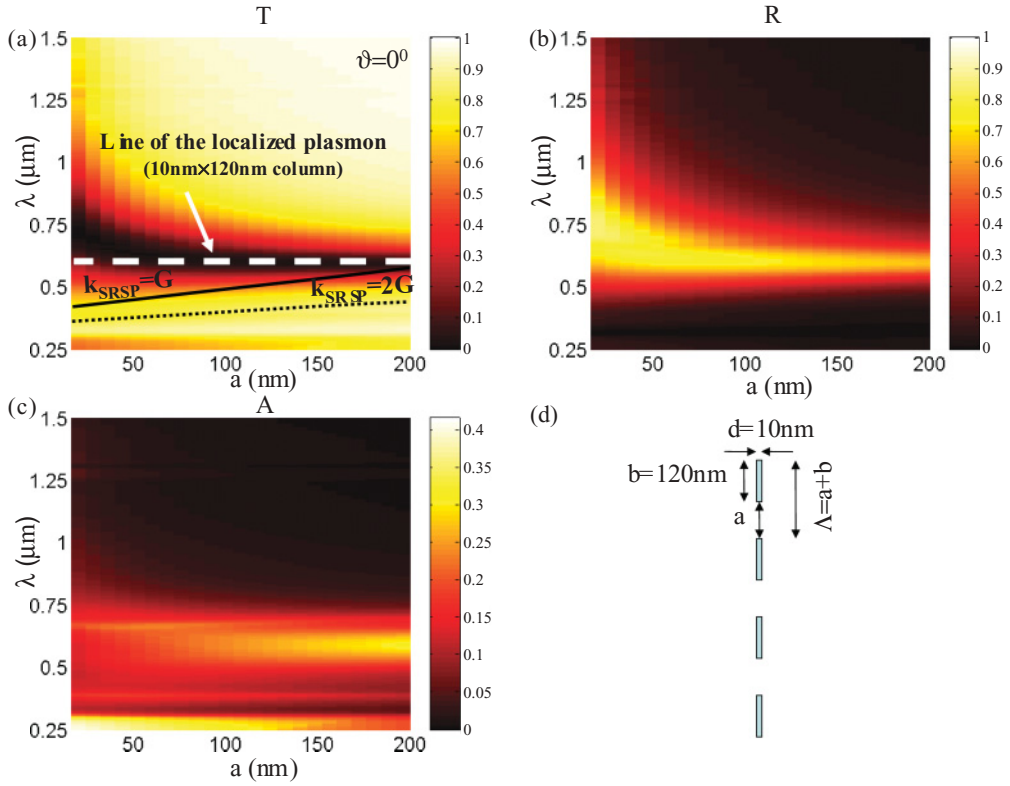

FIG. 7. (Color online) (a)–(c) Transmission (T), reflection (R), and absorption (A) vs slit aperture (a) and incident wavelength (λ) for normal incidence in the case of a grating with thickness $d = 10$ nm and length of the metal in the elementary cell $b = 120$ nm. The corresponding slit aperture is varied from $a = 16$ to 200 nm. The horizontal dashed line in (a) represents the spectral position of the localized plasmon for the 10×120 nm^2 single column. The thin solid and dotted lines represent instead the dispersion of the SRSP coupled respectively with G and $2G$. Note that the frequency of quenched transmission undergoes a redshift with respect to the spectral position of the localized plasmon of the single column as the slit aperture decreases, while on the contrary the dispersion of the SRSP undergoes a blueshift. (d) The grating with the typical dimensions as in Fig. 1(a).

effectively consists of an array of 2D rectangular columns with dimensions b and d and regular period a. We compare in Fig. 5 the absorption for a single building block of such an array with the absorption for the entire grating. The absorption by the single column has been normalized to the power per unit length incident on an elementary cell of the grating, for fair comparison. More explicitly, the absorption of the single column has been calculated as

$$A = \frac{n_{\text{in}}\omega\varepsilon_I \iint_s (|E_x(x,z)|^2 + |E_z(x,z)|^2)dxdz}{\cos(\vartheta)\,\Lambda}, \qquad (4)$$

where n_{in} is the refractive index of the incident medium (air in our case), ε_I is the imaginary part of the electric permittivity of silver as reported in Fig. 1(b), $\omega = 2\pi\nu$ is the pulsation and ν the frequency of operation, E_x and E_z are the two components of the local electric field, and $S = bd$ is the area of the cylinder base. The calculation of the electric fields inside the column has been performed using an analytical procedure that makes use of the Green function for 2D scattering objects as outlined in Refs. 34 and 35.

Figure 5 is very instructive and highlights several relevant features that capture the nature of the quenched transmission phenomenon: the absorption of the grating and the absorption of the single column are qualitatively and quantitatively consistent. In particular, the absorption resonance around 600 nm, directly related to quenched transmission, is well captured by the absorption of the single column. It is well known[30,31,36] that subwavelength metallic objects may support localized surface plasmon resonances at optical frequencies, which drastically increase the absorption cross section of these objects.[37] Unlike planar SPs, which propagate at an air-metal planar interface, localized surface plasmons are nonpropagating resonant oscillations, which lead to field amplification and enhanced scattering and absorption. It is evident from Fig. 5 that the nature of the quenched transmission is strongly related to the excitation of localized surface plasmon resonances at each element of the array, rather than to the photon-LRSP coupling of the entire grating. In fact, the effect of the photon-LRSP coupling is clearly visible [see Figs. 5(b) and 5(c)] in the absorption curves of the grating, due to the presence of spikes characterized by extremely narrow bandwidths, as we have already discussed [see also Fig. 4(c)]. Evidently these spikes have little or nothing to do with the wideband regions of quenched transmission. Moreover, as one may expect, the agreement between the absorption by the single array element and the absorption by the grating gets closer and closer as the mutual distance among columns (i.e., the slit aperture a) becomes larger and larger. This is obviously due to the reduced coupling between the localized plasmons of the columns as their mutual distance increases. The above trend can be clearly

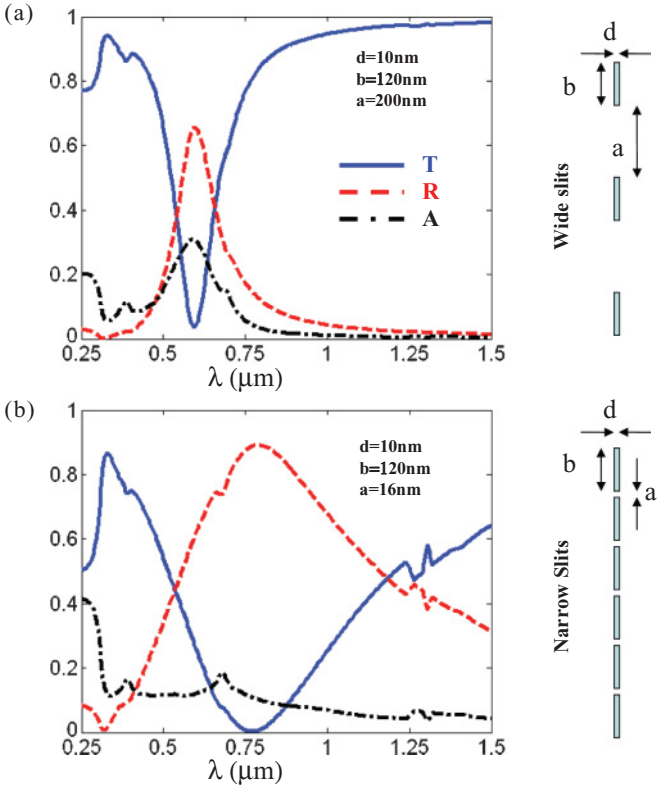

FIG. 8. (Color online) (a) Transmission (T), reflection (R), and absorption (A) vs incident wavelength at normal incidence for slit aperture $a = 200$ nm. (b) Same as in (a) for a slit aperture $a = 16$ nm.

ascertained by looking at Fig. 5(a), where the slit aperture is $a = 200$ nm (continuous line) and 12 μm (dotted line), compared to Fig. 5(d), for which the slit aperture is $a = 600$ nm. In Fig. 5(a) the absorption resonance of the grating with $a = 12$ μm practically coincides with the absorption resonance of the single column, as expected. For fair comparison, the absorption of the grating with $a = 12$ μm has also been normalized to the power per unit length incident on the $\Lambda = 320$ nm period grating. In Fig. 5(d) the vertical arrow indicates a small cusp in the absorption of the grating located at $\lambda = \Lambda = 720$ nm which is the Rayleigh condition[2,3] when the first diffraction order becomes tangent to the grating. We find also that the Rayleigh condition perturbs just slightly the position of the absorption maximum of the grating, making it just weakly deflect from the spectral position of the maximum absorption of the single column. At this point it should be evident that the wideband quenched transmission region can be mainly ascribed to the effect of localized plasmons supported by the single column. Nevertheless, we will give an additional consideration in order to dispel any residual doubt. In Fig. 6 we show the x component of the electric field calculated along the x axis at the center of the grating and compare it with the same field calculated for the case of a single column, as in Fig. 5(a). The incoming plane wave is at normal incidence and its wavelength is 595 nm, which corresponds to the transmission minimum [see Fig. 4(a)]. The figure clearly shows that the field localization inside the single column closely resembles both qualitatively and quantitatively the field localization along the grating, with the small difference associated with weak coupling among the localized plasmon resonances in the array scenario.

In Fig. 7 we investigate in more detail how the quenched transmission depends on the slit aperture a of the grating. In particular, we analyze what happens when we pass from an ultrathin grating with wide slits to an ultrathin grating with very narrow slits. We analyze the grating with $d = 10$ nm, $b = 120$ nm, and a slit aperture that gradually varies from $a = 16$ to 200 nm. From the point of view of the building blocks of the array, varying the slit aperture from 16 to 200 nm corresponds to gradually moving apart the 10×10 nm^2 columns from a side to side distance of $a = 16$ to 200 nm. In terms of air filling factors, the two extreme cases ($a = 16$ and 200 nm) correspond respectively to 5% and 62% air filling factors.

Inspecting Fig. 7, one can easily ascertain that the frequency of quenched transmission is mostly determined by the collective localized surface plasmon resonance of an array of plasmonic columns, whose spectral position is indicated by the dashed horizontal line in Fig. 7(a). For wide slits ($a >$ 100 nm) the localized plasmons of the columns are weakly coupled to each other, while for narrow slits ($a < 100$ nm) they become strongly coupled, producing a broadening of the resonance bandwidth and a typical redshift. In Fig. 7(a) are also reported the corresponding dispersions of the SRSP coupled with G (thin solid line) and $2G$ (dotted line). It is evident that the line of quenched transmission redshifts as the columns get closer and closer, while on the contrary the SRSP dispersions manifest a typical blueshift. This fact is a further proof, if necessary, that SRSPs are not involved in the quenched transmission phenomenon described in this paper. Indeed, for weaker coupling (wider slits) the spectral position of the localized plasmon resonance of the single column describes quite well the frequency and amplitude of the quenched transmission effect. As the coupling among columns increases (thinner slits), the localized plasmons become more strongly coupled to each other, resulting in a redshift of the zone of quenched transmission accompanied by an increase in reflection, and corresponding decrease in absorption. The two regimes are epitomized in Fig. 8, where we show the two extreme cases with $a = 200$ and 16 nm for the same geometry of the single column, corresponding respectively to weak and strong coupling of localized plasmon resonances.

Figure 8 in particular highlights how in the weak-coupling regime (wide slits) the resonance of the suppressed transmission is centered at 595 nm, while in the strong-coupling regime (narrow slits) the resonance enlarges and redshifts with the minimum located at 750 nm. This resonance shift is simply due to the coupling among the closely spaced resonators, and it is a typical phenomenon in strongly coupled resonant systems, and plasmonic arrays in particular.[38] The increase in reflection and decrease in absorption that take place in the highly coupled regime represent a typical screening and quenching effect due to the large array coupling, which produces an overall reduction of field enhancements in each element of the array when the coupling gets larger.[39] It is evident from these results that the effect of quenched transmission can be directly associated with the collective resonance of the localized plasmons supported by each element of the grating.

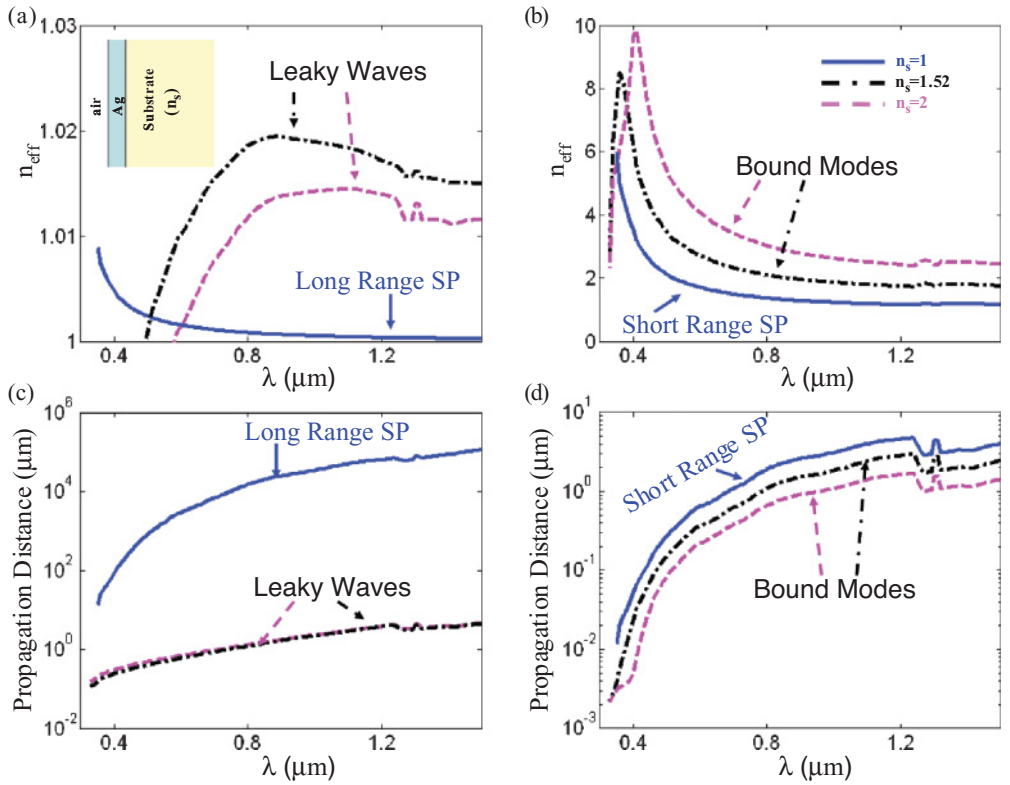

FIG. 9. (Color online) (a) Real part of the effective index of the LRSP and of the corresponding leaky waves vs wavelength for a structure air/Ag(10 nm)/n_s with $n_s = 1$ (continous line), 1.52 (dash-dotted line), and 2 (dashed line). In the inset the structure under investigation is schematically represented. (b) Real part of the effective index of the SRSP and of the corresponding bound modes vs wavelength for a structure air/Ag(10 nm)/n_s with $n_s = 1$ (continous line), 1.52 (dash-dotted line), and 2 (dashed line). (c) Propagation distance for the modes reported in (a). (d) Propagation distance for the modes reported in (b).

In our analysis, for the sake of simplicity, we have studied the case of a free-standing grating, i.e., air/grating/air. In the optical regime, from an experimental point of view the metal strips will be likely deposited on a glass substrate, which may slightly modify these results.[15] We do not predict large modifications in these discussions due to the presence of a substrate, as discussed in the following. We specifically confirm this prediction in Fig. 9, where we study the guided modes supported by a structure air/Ag(10 nm)/n_s where n_s is the refractive index of the substrate, which here for simplicity is considered nondispersive. In particular, we compare three cases: $n_s = 1$, 1.52, and 2. In agreement with previous studies,[28] we find that the LRSP of the symmetric structure air/Ag(10 nm)/air becomes a leaky wave for the asymmetric structure air/Ag(10 nm)/n_s, with leakage taking place in the substrate. This causes a dramatic decrease of the leaky wave propagation length, which becomes comparable with the propagation length of the SRSP of the symmetric structure air/Ag(10 nm)/air. In contrast, the SRSP of the symmetric structure remains somewhat less affected by the introduction of the substrate; it still remains a bounded mode with a short propagation distance, comparable to that of the SRSP of the symmetric structure. The final conclusion is that the introduction of the substrate essentially prevents any efficient coupling of planar SPs with the grating.

It is now left to investigate how the introduction of a substrate affects the wideband zone of quenched transmission. This issue is explored in Fig. 10, where we see that the zone of quenched transmission redshifts when the refractive index of the substrate is increased; this holds true both at normal [see Fig. 10(a)] and at oblique incidence [see Fig. 10(b)]. Moreover, we note from Fig. 10(b) that the narrowband quenched transmission due to the coupling of the LRSP with the grating actually disappears when we introduce the substrate. This feature can be easily explained by the fact that, as shown above, the LRSP becomes a leaky mode, worsening the coupling efficiency with the grating.

In Figs. 11(a) and 11(b) we compare the absorption of the single column at normal incidence with the absorption of the entire grating in the presence of the substrate, analogously to Fig. 5. The redshift of the absorption resonance as the refractive index of the substrate increases continues to hold true both for the grating and for the single column in similar proportion. The redshift in the localized SP resonance due to the presence of a substrate was predicted and experimentally confirmed in Ref. 40. The redshift of the transmission minimum due to a substrate as shown in Fig. 11 is another strong indication of the dominant role played by the localized surface plasmons in the quenched transmission.

III. CONCLUSIONS

In conclusion, we have analyzed here the phenomenon of quenched transmission in ultrathin, subwavelength, plasmonic

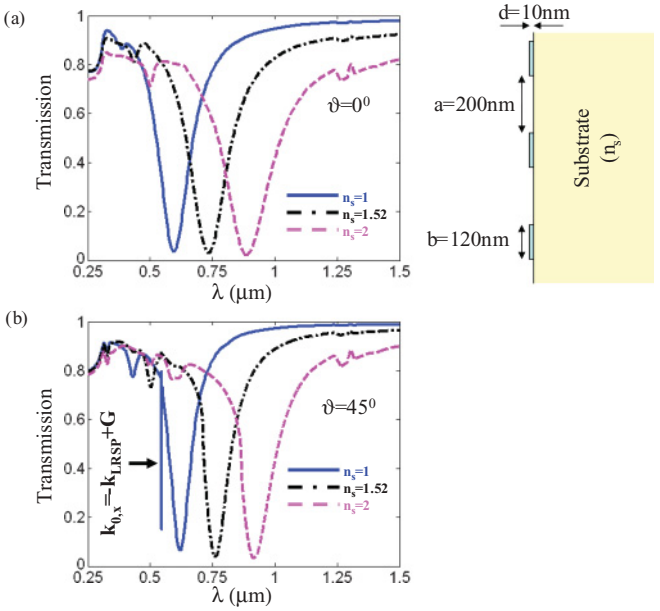

FIG. 10. (Color online) (a) Transmission vs wavelength at normal incidence for different values of the refractive index of the substrate. The dimensions of the grating are the same as the one described in Fig. 3. (b) Transmission vs wavelength at 45° incidence. The arrow indicates the narrowband region of quenched transmission that is due to the coupling of the LRSP with the grating in the symmetric structure air/grating/air. The introduction of the substrate washes out this narrow resonance because the LRSP becomes a leaky wave, and its efficient coupling with the grating is no longer possible.

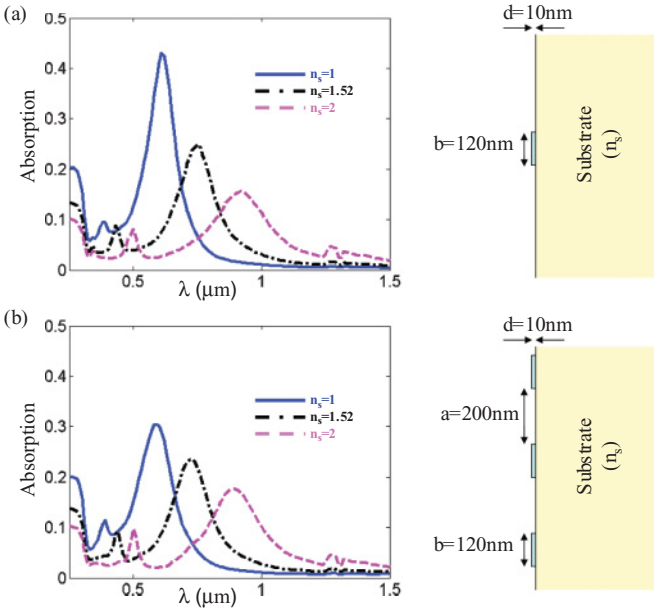

FIG. 11. (Color online) (a) Normalized absorption at normal incidence of the single column for different refractive indices of the substrate. (b) Normalized absorption at normal incidence of the grating for different refractive indices of the substrate.

gratings. In particular, we have shown that this anomalous effect is mainly due to the excitation of localized surface plasmon resonances supported by the building blocks of the grating (metallic columns in the geometry analyzed here). The localized plasmons may be either strongly or weakly coupled, depending on the slit aperture in the grating, but their collective resonant behavior mainly determines the quenched transmission and enhanced absorption. We have clearly demonstrated that SRSPs play a negligible role in this effect, due to their extremely short propagation distance, while LRSPs may contribute to additional extremely sharp resonances similar to Wood's anomalies,[1] without, however, directly producing the quenching effect. Moreover, the introduction of a substrate washes out even these sharp resonances because the LRSP becomes a leaky wave,[28] preventing any efficient coupling with the grating. We believe that the quenched transmission phenomenon may have several interesting applications, e.g., for compact light-polarizer devices. It could also be very intriguing to study such gratings when loaded with nonlinear, Kerr-like, material inclusions, in order to realize efficient, ultracompact, all-optical switching devices. We believe that the present study may provide a better understanding of the quenched transmission phenomenon, leading to its possible use in practical applications.

*giuseppe:daguanno@us.army.mil

[1] R. W. Wood, Philos. Mag. **4**, 396 (1902).
[2] F. J. García de Abajo, Rev. Mod. Phys. **79**, 1267-1286 (2007).
[3] F. J. Garcia-Vidal, L. Martin-Moreno, T. W. Ebbesen, and L. Kuipers, Rev. Mod. Phys. **82**, 729 (2010).
[4] R. Magnusson and S. S. Wang, Appl. Phys. Lett. **61,** 1022 (1992).
[5] S. Fan and J. D. Joannopoulos, Phys. Rev. B **65**, 235112 (2002).
[6] G. D'Aguanno, N. Mattiucci, M. J. Bloemer, D. de Ceglia, M. A. Vincenti, and A. Alù, J. Opt. Soc. Am. B **28**, 253 (2011).
[7] A. A. Oliner and D. R. Jackson, in *Digest of the 2003 IEEE Antennas and Propagation Society International Symposium* (Columbus, OH, 2003), Vol. 2, pp. 1091–1094.
[8] A. Alù, F. Bilotti, N. Engheta, and L. Vegni, IEEE Trans. Antennas Propag. **AP-54**, 1632 (2006).
[9] A. Yariv and P. Yeh, *Optical Waves in Crystals* (John Wiley & Sons, New York 1984).
[10] Dale C. Flanders, Appl. Phys. Lett. **42,** 492 (1983).
[11] B. Schnabel, E.-B. Kley, and F. Wyrowski, Opt. Eng. **38,** 220 (1999).
[12] Y. Ekinci, H. H. Solak, C. David, and H. Sigg, Opt. Express **14,** 2323 (2006).
[13] E. D. Palik, *Handbook of Optical Constants of Solids* (Academic Press, New York, 1991).
[14] I. S. Spevak, A. Yu. Nikitin, E. V. Bezuglyi, A. Levchenko, and A.V. Kats, Phys. Rev. B **79,** 161406(R) (2009).
[15] S. Xiao, J. Zhang, L. Peng, C. Jeppesen, R. Malureanu, A. Kristensen, and N. A. Mortensen, Appl. Phys. Lett. **97,** 07116 (2010).

[16]J. Braun, B. Gompf, G. Kobiela, and M. Dressel, Phys. Rev. Lett. **103**, 203901 (2009).
[17]S. G. Rodrigo, L. Martin-Moreno, A. Yu. Nikitin, A. V. Kats, I. S. Spevak, and F. J. Garcia-Vidal, Opt. Lett. **34**, 4 (2009).
[18]P. Lalanne and G. M. Morris, J. Opt. Soc. Am. A **13**, 779 (1996).
[19]G. Granet and B. Guizal, J. Opt. Soc. Am. A **13**, 1019 (1996).
[20]L. Li, J. Opt. Soc. Am. A **13**, 1870 (1996).
[21]Robert J. Marks II, *Introduction to Shannon Sampling and Interpolation Theory* (Springer-Verlag, New York, 1991).
[22]H. A. Macleod, *Thin Film Optical Filters* (Institute of Physics Publishing, Bristol and Philadelphia, 2001).
[23]S. Ciraci and I. P. Batra, Phys. Rev. B **33**, 4294 (1986).
[24]A. I. Maaroof and D. S. Sutherland, J. Phys. D **43**, 405301 (2010).
[25]T. Okamoto, K. Kakutani, T. Yoshizaki, M. Haraguchi, and M. Fukui, Surf. Sci. **544**, 67 (2003).
[26]V. P. Drachev, U. K. Chettiar, A. V. Kildishev, H.-K. Yuan, W. Cai, and V. Shalaev, Opt. Express **16**, 1186 (2008).
[27]D. Sarid, Phys. Rev. Lett. **47**, 1927 (1981).
[28]J. J. Burke, G. I. Stegeman, and T. Tamir, Phys. Rev. B **33**, 5186 (1986).
[29]N. Mattiucci, G. D'Aguanno, and M. J. Bloemer, Opt. Express **18**, 23698 (2010).
[30]H. Raether, *Surface Plasmons*, Springer Tracts in Modern Physics (Springer, Berlin, 1988).
[31]S. A. Maier, *Plasmonics: Fundamentals and Applications* (Springer, Berlin, 2007).
[32]U. Fano, Phys. Rev. **124,** 1866 (1961).
[33]A. E. Miroshnichenko, S. Flach, and Y. S. Kivshar, Rev. Mod. Phys. **82**, 2257 (2010).
[34]A. D. Yaghjian, Proc. IEEE **68**, 248 (1980).
[35]O. J. F. Martin and N. B. Piller, Phys. Rev. E **58,** 3909 (1998).
[36]M. J. Bloemer, T. L. Ferrell, M. C. Buncick, and R. J. Warmack, Phys. Rev. B **37,** 8015 (1988).
[37]C. F. Bohren, Am. J. Phys. **51**, 323 (1983).
[38]A. Alù, and N. Engheta, in *Structured Surfaces as Optical Metamaterials*, edited by A. A. Maradudin (Cambridge University Press, Cambridge, in press).
[39]P. Anger, P. Bharadwaj, and L. Novotny, Phys. Rev. Lett. **96**, 113002 (2006).
[40]P. Royer, J. P. Goudonnet, R. J. Warmack, and T. L. Ferrell, Phys. Rev. B **35,** 3753 (1987).